

# Optimization of loop-network reconfiguration strategies to eliminate transmission line overloads in power system restoration process with wind power integration

Shaoyan Li<sup>a,\*</sup>, Liyuan Wang<sup>a,b</sup>, Xueping Gu<sup>a</sup>, Hanguang Zhao<sup>a</sup>, Yongzhao Sun<sup>a</sup>

<sup>a</sup> School of Electrical and Electronic Engineering, North China Electric Power University, Hebei 071003, China

<sup>b</sup> State Grid Changfeng County Electric Power Supply Company, Hefei 231131, China

## ARTICLE INFO

### Keywords:

Network reconfiguration  
Power system restoration  
Transmission line overloads  
Wind power penetration  
Mixed-integer nonlinear programming

## ABSTRACT

With large-scale wind power integration, the uncertainty of the wind power outputs will aggravate the transmission line overloads during the black-start restoration process. By constructing regional loop-networks, this paper proposes an optimization method of network reconfiguration strategies to eliminate the line overloads. Firstly, a multi-scenario set of the wind power outputs is constructed based on the extreme scenario method. Secondly, a loop-network reconfiguration optimization model is established to meet the requirements of the multi-scenario set simultaneously, where the line overloads are not permitted. Then, a two-layer solving framework is proposed to solve the optimization model. The upper-level layer is a multi-scenario mixed integer linear programming (MILP) model with the DC power flow constraints, whose objective is to minimize the operation complexity index. The lower-level layer serves to check the standing phase angle (SPA) constraint and the AC power flow constraints of the optimal schemes obtained from the upper-level layer. Therefore, the loop-network reconfiguration optimization model is alternatively solved by iterative computation. The effectiveness of the proposed method is verified by the modified IEEE 39-bus system and the modified IEEE 118-bus system, and applicability of this method to practical systems is verified by the southwestern Yunnan power system in China.

## 1. Introduction

In recent years, due to the shortage of traditional fossil-fuel energy, wind power as a representative of clean and renewable energy has attracted worldwide attention [1,2]. The integration of large-scale wind power into the power network has brought many challenges to power systems. Due to the uncertainty of wind power output, the system stability and security are seriously endangered, and the risk of major blackout accidents is also increased. It is necessary to work out a black start scheme considering the large-scale wind power integration.

Power system restoration is a complex issue with multiple targets, constraints, and variables. Normally, the system restoration is divided into three stages: a) black start, b) network reconfiguration and c) load restoration [3]. Whereas, with the rapid development of wind power, the power system restoration with wind power integration has become an urgent issue to be studied. Currently, the beneficial explorations on which wind power integrates into system restoration include: wind power as a black-start power [4], wind power participating in network

reconstruction [5], and wind power participating in load restoration [6,7], etc. In the restoration process, network reconfiguration is one of the important tasks to restore the backbone grid as soon as possible. The existing researches about network reconfiguration mainly focus on the optimization of the restoration paths [8,9], determination of the target network structures [10], optimization of the unit restoration sequences [11,12] and system partitioning for parallel restoration [13]. However, the network structure during the reconfiguration process is usually radial [14]. In this structure, transmission line overloads are more likely to occur due to the wind power uncertainty. It seriously threatens the system security and delays the restoration process. For instance, during the restoration process of the “11.4” blackouts in Europe in 2006 [15], the integration of large-scale wind power into the system caused the transmission line overloads and resulted in a secondary power outage. Therefore, in order to improve the network security and reliability in the reconfiguration process, it is necessary to eliminate the possible line overloads in the case of large-scale wind power integration.

In the fields of preventive control and corrective control of normal operation, the line overloads are generally eliminated by adjusting unit

\* Corresponding author.

E-mail address: [shaoyan.li@ncepu.edu.cn](mailto:shaoyan.li@ncepu.edu.cn) (S. Li).

<https://doi.org/10.1016/j.ijepes.2021.107351>

Received 5 February 2021; Received in revised form 8 May 2021; Accepted 30 June 2021

Available online 21 August 2021

0142-0615/© 2021 Elsevier Ltd. All rights reserved.

**Nomenclature****Indices**

$i, j$	Node number
$c$	Circuit line number
$g$	Unit index
$w$	Wind farm index
$s$	Wind power output scenario index
$t$	Time index
$l$	Iteration index

**Parameters**

$\alpha$	Confidence level
$n$	Number of the wind farms
$n_{\text{node}}$	Number of the system nodes
$b_{ijc}, g_{ijc}, x_{ijc}$	Charging susceptance, conductance and reactance of line $i$ - $j$ - $c$
$b_{\text{base}}$	Charging susceptance reference value of line $i$ - $j$ - $c$
$\mu_w, \sigma_w$	Mean and standard deviation of wind farm $w$ output
$E(P_{w,t}^{\text{pre}}), V(P_{w,t}^{\text{pre}})$	Expectation and variance of wind farm $w$ output
$P_{w,t}^{\text{min}}, P_{w,t}^{\text{max}}$	Minimum and maximum output of wind farm $w$ at time $t$
$P_{1,t}^{\text{act}}, P_{2,t}^{\text{act}}$	Actual active power output of wind farm 1 and wind farm 2 at time $t$
$\bar{P}_1, \bar{P}_2$	Active power mean value of wind farm 1 and wind farm 2 during time $T$
$r$	Correlation coefficient between two wind farms outputs
$k_1$	Weight coefficient, with a value greater than 1
$k_2$	Weight coefficient, with a value less than 1
$F_{\text{loop}}$	Loop-closing operation number
$F_{\text{ope}}$	Operation complexity index
$f$	Objective function (Operation complexity index)
$J$	Maximum number of allowable lines
$M$	Large positive real number
$P_g^{\text{min}}, P_g^{\text{max}}$	Maximum and minimum active power output of unit $g$
$Q_g^{\text{min}}, Q_g^{\text{max}}$	Maximum and minimum reactive power output of unit $g$
$P_g^{\text{fixed}}$	Fixed output of non-black-start unit $g$
$P_{ijc}^{\text{min}}, P_{ijc}^{\text{max}}$	Upper and lower limits of active power flow on line $i$ - $j$ - $c$
$Q_{ijc}^{\text{min}}, Q_{ijc}^{\text{max}}$	Upper and lower limits of reactive power flow on line $i$ - $j$ - $c$
$v_i^{\text{min}}, v_i^{\text{max}}$	Upper and lower limit of voltage amplitude at node $i$
$\theta_i^{\text{min}}, \theta_i^{\text{max}}$	Upper and lower limit of voltage phase at node $i$
$\theta_{\text{set}}$	Phase setting of the system synchronous detection relay for loop-closing operation
$N_{\theta, \text{infeas}}^{s,l}$	Sum of angle variable matrix in scene $s$ and iteration $l$ . If $N_{\theta, \text{infeas}}^{s,l} = 1$ , the solution is infeasible.
$\hat{z}_{ijc}$	Combinatorial representation of the optimal network

obtained from the upper-level layer model

**Variables**

$z_{ijc}$	Binary decision variable characterizing whether line $i$ - $j$ - $c$ is in the target network. If yes, values 1, otherwise, values 0
$m_i$	Binary decision variable whether node $i$ is restored. If yes, values 1, otherwise, values 0
$P_{ijc,t}^s, Q_{ijc,t}^s$	Active and reactive power flow through line $i$ - $j$ - $c$ at time $t$ in scene $s$
$P_{g,t}^s, Q_{g,t}^s$	Active and reactive power of unit $g$ at time $t$ in scene $s$
$P_{di,t}, Q_{di,t}$	Active and reactive load of node $i$ at time $t$
$v_{i,t}^s, v_{j,t}^s$	Voltage amplitude of node $i$ and node $j$ at time $t$ in scene $s$
$\theta_{i,t}^s, \theta_{j,t}^s$	Voltage phase of node $i$ and node $j$ at time $t$ in scene $s$
$\theta_{ij,t}^s$	Phase difference between node $i$ and node $j$ at time $t$ in scene $s$
$P_{w,t}^{\text{pre}}$	Predicted output of wind farm $w$ at time $t$
$P_w^{\text{pre}}$	Maximum or minimum of predicted output of wind farm $w$

**Sets**

$L$	Set of all lines
$L^{\text{to}}$	Set of the outflow lines
$L^{\text{from}}$	Set of the inflow lines
$L_{\text{en}}$	Set of recovered lines
$L_{\text{un}}$	Set of to-be-recovered lines
$N$	Set of all nodes
$N_{\text{en}}$	Set of the charged nodes
$N_{\text{un}}$	Set of the uncharged nodes
$G$	Set of all units
$G_{\text{BS}}$	Set of the black-start unit
$W$	Set of all wind farms
$S$	Multi-scenario set of wind power
$T$	Set of wind power output time
$E_l$	Set of to-be-recovered lines obtained by the upper-level model in an iteration of the previous $l$ iterations
$D_w$	Uncertain output set of the wind farm $w$
$K_l$	Dynamic set, on the first iteration $K_l = \Phi$ , then the subsequent iterations $K_l = K_{l-1} \cup E_{l-1}$
$N_{\text{re}}^{s,l}$	Set of the charged nodes determined by the iteration $l$ of MILP model

**Matrix**

$R$	Correlation coefficient matrix of wind power outputs
$A_{N \times N}^s$	Variable matrix in scene $s$
$I_{N \times N}^{s,l}$	Adjacency matrix in scene $s$ and iteration $l$
$C_{N \times N}^{s,l}$	Reachability matrix in scene $s$ and iteration $l$
$A_{\text{temp}}^{s,l}$	Intermediate variable matrix in scene $s$ and iteration $l$

outputs or node loads [16,17], rather than changing the network structure. However, the primary target of system restoration is to restore the unit outputs and user's loads as soon as possible. So to eliminate line overloads, it is better to adjust network structure than to adjust unit outputs or shed load. Currently, optimal transmission switching (OTS) is adopted to enhance the system security by alleviating line overloads [18,19] or voltage limit violation [19]. It can also be employed to improve the operation economy of power systems [20,21] and increase the network-connected capacity of wind power [22,23]. Due to its merits, much attention has been paid to OTS in Europe [24]. OTS can be utilized to construct regional loop-networks to eliminate transmission line overloads in the restoration process, as an effective measure of network control.

During loop-network reconfiguration, more attention has been paid to the coordination of load recovery and unit outputs [25], and

adjustment of SPA constraint for loop-closing operation by means of load recovery control under a fixed network structure. Reference [26] proposed an optimization model for the loop-network reconfiguration. However, it needs to adjust the unit outputs and node loads to meet the SPA constraint. Reference [27] proposed a loop-network reconfiguration strategy to eliminate the line overloads by establishing an mixed-integer nonlinear programming model (MINLP) considering AC power flow constraints. However, the uncertainty of the wind power outputs is not considered in the MINLP model.

Although there are many researches on wind power participating in system restoration and loop-network reconfiguration, it is still worth studying the optimization strategy of loop-network reconfiguration considering wind power integration. Therefore, on basis of the existing work, this paper proposes an optimization strategy for loop-network reconfiguration to eliminate line overloads. Firstly, a loop-network

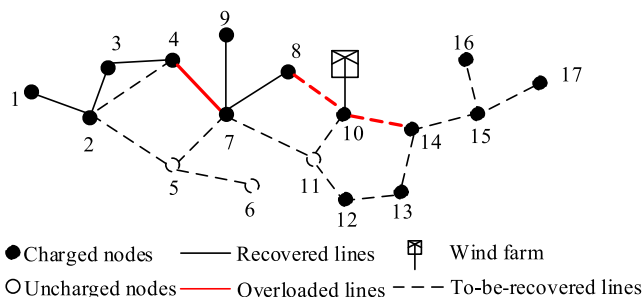


Fig. 1. Schematic diagram of loop-network construction.

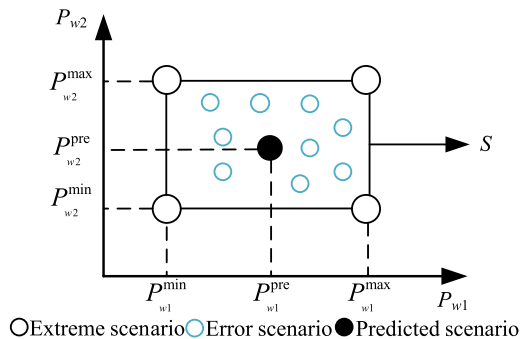


Fig. 2. Illustration of extreme scenarios.

reconfiguration strategy is proposed, and a multi-scenario set depicting the uncertainty of wind power outputs is built based on extreme scenario method. Secondly, a MINLP model, which meets the multi-scenario set constraints and AC power flow constraints, is established for network topology optimization. To facilitate solving the MINLP model, a two-layer alternative solving method is applied. The upper-level layer is a multi-scenario mixed-integer linear programming (MILP) model considering the DC power flow constraints for line overloads elimination. The lower-level layer serves to check the SPA constraint and the AC power flow constraints of the optimal schemes obtained by the upper-level layer model by solving a non-linear programming (NLP) problem. A commercial solver is employed to solve the optimization model. Therefore, the optimal loop-network reconfiguration strategy is obtained by iterative computation, in which two layers models are solved alternatively. The modified IEEE 39-bus system and IEEE 118-bus system examples are used to verify effectiveness of the proposed optimization method. The southwestern Yunnan power system in China, a provincial transmission network, is taken as an instance to verify applicability of the proposed method to practical systems.

The contributions of this paper are summarized as follows:

- An optimization strategy of loop-network reconfiguration is proposed considering wind power output characteristic to eliminate line overloads.
- A MINLP model is established to eliminate line overloads for multi-scenario set considering AC power flow constraints.
- An effective two-layer solving framework is proposed to solve the established MINLP model by an alternative and iterative calculating process.

The rest of this paper is organized as follows. In Section 2, a loop-network reconfiguration strategy is addressed. On this basis, the factors affecting the elimination of line overloads in network reconfiguration are discussed. The uncertainty model of wind power outputs is established in Section 3 and the optimization model for loop-network reconfiguration under different wind power output scenarios is established in Section 4. In Section 5, the two-layer solving framework of the

established MINLP model is described. Section 6 shows the test results of the proposed method in the modified IEEE 39-bus system and modified IEEE 118-bus system examples. Concluding remarks are given in Section 7.

## 2. Loop-network reconfiguration strategy to eliminate transmission line overloads

### 2.1. Proposal of loop-network reconfiguration strategy

There are many uncertain factors during the network reconfiguration process. The radical-structure network determined by the traditional restoration scheme is relatively fragile, which may cause some operation problems such as transmission line overloads. Due to the uncertainty of wind power outputs, large-scale wind power participating in network reconfiguration tends to exacerbate line overloads. Therefore, building loop-networks through flexible loop-closing operation can reduce the load ratio of the overloaded lines. The schematic diagram of the loop-network construction is shown in Fig. 1.

In Fig. 1, node 1 is connected to the sending-end (source) and node 17 to the receiving-end (load) of the system. A wind farm is connected to node 10, and the uncertain power output of the wind farm exacerbates the overloads of line 4–7, line 8–10 and line 10–14. In this case, adding some lines represented by the dashed lines in Fig. 1 to construct loop-network can effectively alleviate the overloading problem and enhance the operation security.

### 2.2. Considered factors of a loop-network reconfiguration strategy

Two factors are considered for formulating a loop-network reconfiguration strategy.

- Uncertainty of wind power outputs which requires proper modeling method.
- Selection of the available lines for constructing loop-network to alleviate the line overloads.

Meanwhile, the loop-network construction process generally requires loop-closing operation. When the loop-closing operation is carried out, the phase angle difference between two sides of the connecting points of the loop-network must be less than the set value. Otherwise, the nearby equipment may be damaged; or even worse, the blackouts may recur.

## 3. Uncertainty model of wind power output

So far, there have been some studies on the uncertainty model of wind power outputs, including the scenario analysis method [28,29], chance-constrained programming [22,30], robust optimization method [31] and so on. However, the former two methods have some limitations due to the huge calculation amount or probabilistic distribution function. Comparatively speaking, the robust optimization method has certain superiority and has been applied on the load restoration considering individual subsystems under uncertain conditions [32]. The extreme scenario method [33] is applied to construct a value space through typical extreme scenarios. As long as the boundary extreme scenarios under severe conditions can meet all constraints, so can all the scenarios in the value space, which is basically consistent with the essence of robust optimization. Thus, the extreme scenario method is required to construct a multi-scenario set of wind power outputs to describe the wind power uncertainty properly.

### 3.1. Extreme scenario method

As the short-term prediction error of wind power is as high as 25%–40% [34], it is of significance to deal with the wind power uncertainty properly. Fig. 2 is a schematic of the extreme scenarios. Each vertex of the rectangle represents an extreme scenario where the power output of

each wind farm is at its upper or lower limit value. When the number of wind farms is two, the number of extreme scenarios is  $2^2$ , and the value space  $S$  is a two-dimensional rectangle. Similarly, when the number of wind farms is  $n$ , the number of extreme scenarios is  $2^n$ . Accordingly, the value space  $S$  is an  $n$ -dimensional geometric body.

### 3.2. Determination of the wind power multi-scenario set

The extreme scenarios of wind power output are typical, and the uncertainty set should include all outputs of each single wind power. Compared with the predicted scenario, the smaller the value space  $S$ , the fewer error scenario included, and the lower the reliability of the optimal solution. Therefore, the uncertainty set of each single wind farm is described by Eq. (1), which is equivalent to the chance-constrained equation at the confidence level  $\alpha$ , as shown by Eq. (2).

$$D_w = \left\{ P_{w,t}^{\text{pre}} \mid P_{w,t}^{\text{min}} \leq P_{w,t}^{\text{pre}} \leq P_{w,t}^{\text{max}} \right\} \quad (1)$$

$$\Pr\left(P_{w,t}^{\text{min}} \leq P_{w,t}^{\text{pre}} \leq P_{w,t}^{\text{max}}\right) \geq 1 - \alpha \quad (2)$$

Since multiple wind farms have correlation in time and space, the linear correlation coefficient  $r$  is used to characterize the correlation degree between two wind farms outputs [35], described by Eq. (3). It constitutes the correlation coefficient matrix  $R$  of multiple wind farms, as shown by Eq. (4).

$$r_{12} = \frac{\sum_{t=1}^T (P_{1,t}^{\text{act}} - \bar{P}_1)(P_{2,t}^{\text{act}} - \bar{P}_2)}{\sqrt{\sum_{t=1}^T (P_{1,t}^{\text{act}} - \bar{P}_1)^2} \sqrt{\sum_{t=1}^T (P_{2,t}^{\text{act}} - \bar{P}_2)^2}} \quad (3)$$

$$R = \begin{bmatrix} 1 & r_{12} & \cdots & r_{1n} \\ r_{21} & 1 & \cdots & r_{2n} \\ \vdots & \vdots & \ddots & \vdots \\ r_{n1} & r_{n2} & \cdots & 1 \end{bmatrix} \quad (4)$$

Reference [36] proposed a method to construct the uncertainty set. According to it, the upper and lower output limit values of the wind farms can be obtained at the confidence level  $\alpha$ .

Firstly, the expected value and variance of multiple wind farms outputs are given by Eq. (5).

$$\begin{cases} E(P_{w,t}^{\text{pre}}) = \sum_{w=1}^n \mu_{w,t} \\ V(P_{w,t}^{\text{pre}}) = \sum_{w=2}^n r_{1w} \sigma_{1,t} \sigma_{w,t} + \sum_{w=3}^n r_{2w} \sigma_{2,t} \sigma_{w,t} \\ \quad + \cdots + r_{(n-1)n} \sigma_{n-1,t} \sigma_{n,t} \end{cases} \quad (5)$$

Secondly, it is supposed that the probability density function of wind power output has one single peak, and the expressions of the upper and lower limits are also different under different confidence levels. When  $0 \leq \alpha \leq 1/3$  and  $1/3 \leq \alpha \leq 1$ , the expressions are given by Eqs. (6) and (7) respectively.

$$\begin{cases} P_{w,t}^{\text{min}} = E(P_{w,t}^{\text{pre}}) - \frac{2}{3} \sqrt{\alpha^{-1} V(P_{w,t}^{\text{pre}})} \\ P_{w,t}^{\text{max}} = E(P_{w,t}^{\text{pre}}) + \frac{2}{3} \sqrt{\alpha^{-1} V(P_{w,t}^{\text{pre}})} \end{cases} \quad (6)$$

$$\begin{cases} P_{w,t}^{\text{min}} = E(P_{w,t}^{\text{pre}}) - (1 - \alpha) \sqrt{3V(P_{w,t}^{\text{pre}})} \\ P_{w,t}^{\text{max}} = E(P_{w,t}^{\text{pre}}) + (1 - \alpha) \sqrt{3V(P_{w,t}^{\text{pre}})} \end{cases} \quad (7)$$

After obtaining the upper and lower limits of a single wind power output, the typical extreme scenarios are constructed by freely

combining the upper and lower limits of the multiple wind farms outputs. Then a multi-scenario set of wind power output is determined. In fact, the determination of the extreme scenarios is made up of the vertices of the hypercube representing the variation range of wind power output. Thus, the multi-scenario set of wind power output is shown in Eq. (8).

$$S = \left\{ (P'_1, \dots, P'_w, \dots, P'_n) \mid P'_w = \underset{t=0}{\overset{t=T}{\max}} P_{w,t}^{\text{pre}} \text{ or } P'_w = \underset{t=0}{\overset{t=T}{\min}} P_{w,t}^{\text{pre}} \right\} \quad (8)$$

## 4. Optimization Model of loop-network reconfiguration for multi-scenario set

### 4.1. Definition of objective function

The to-be-restored lines and the to-be-charged nodes are used as the control variables. In this paper, an index representing the complexity of restoration operation is defined and taken as the optimization objective. The optimization model of loop-network reconfiguration is obtained by minimizing the operation complexity index.

#### a) Linear expression of the loop-closing operation number

Based on the electric network theory [37], the linear and analytic mapping relationship can be obtained between the loop-closing operation number and the decision variables, as follows:

- 1) In a circuit with  $N_{\text{node}}$  nodes and  $N_{\text{line}}$  branches, the number of branches of any tree is  $N_{\text{node}} - 1$  and the number of connected branches is  $N_{\text{line}} - N_{\text{node}} + 1$ .
- 2) A circuit with only one connected branch is called the basic circuit. The number of basic circuits is equal to the number of connected branches  $N_{\text{line}} - N_{\text{node}} + 1$ .

Obviously, the loop-closing operation number is equal to the number of independent loops in a target network, and the number of independent loops is equal to the number of basic loops in the network. Therefore, the linear expression of the loop-closing operation number is derived and shown in Eq. (9).

$$F_{\text{loop}} = \sum_{(i,j,c) \in L} z_{ijc} - \sum_{i \in N} m_i + 1 \quad (9)$$

It can be seen from Fig. 1 that the number of the nodes denoted by  $N_{\text{node}}$  is 17, and the total number of the lines denoted by  $N_{\text{line}}$  is 20. Then the number of the independent loops denoted by  $N_{\text{loop}}$  is 4, that is, the loop-closing operation number is 4, which verifies correctness of Eq. (9).

#### b) Definition of operation complexity index

As for the line overloads elimination, new lines need to be added to the radial network. In addition, due to the great impact on the system, the loop-closing operation number should be reduced as far as possible. Therefore, the weighted sum of the newly restored transmission line number and loop-closing number is defined as the operation number. Since the loop-closing operation is more complicated than the line charging operation, the weight coefficient  $k_1$  is greater than 1 as a penalty term, as shown in Eq. (10).

$$F_{\text{ope}} = \sum_{(i,j,c) \in L_{\text{un}}} z_{ijc} + k_1 \left( \sum_{(i,j,c) \in L} z_{ijc} - \sum_{i \in N} m_i + 1 \right) \quad (10)$$

When the wind power participates in network reconfiguration, over-voltage problems may occur at low-load level due to lines charging reactive power. Therefore, it is necessary to make the charging reactive power of new lines as small as possible. The operation number in Eq. (10) should also be reduced as far as possible. As a result, the objective

function, named as operation complexity index, is defined as the weighted sum of the following two terms: the charging reactive power of the newly restored lines and the operation number. The analytical expression of the operation complexity index is given by Eq. (11).

$$f = F_{\text{ope}} + k_2 \sum_{(i,j,c) \in L_{\text{un}}} z_{ijc} \frac{b_{ijc}}{b_{\text{base}}} \quad (11)$$

In the middle or later stages of restoration, the capability of leading-phase operation of the power system will increase, therefore the coefficient  $k_2$  should be decreased accordingly.

#### 4.2. MINLP model to eliminate line overloads for multi-scenario set considering AC power flow constraints

When the restored loop-network based on the optimal scheme deals with the worst scenario, the scheme can guarantee the full adaptability to all scenarios. However, the wind farms are expected to have different outputs when they are connected to different locations. When a wind farm is connected to the receiving-end, the closer the expected wind power output is to the lower limit, the worse the scenario is. Nevertheless, when it is difficult to distinguish the sending-end and receiving-end of the network, the worst scenario cannot be determined directly from the wind power outputs. In the light of this, a multi-extreme-scenario set of the wind power outputs is created in this paper, so as to obtain the optimal solution satisfying requirements of all the possible scenarios.

The optimization model of loop-network reconfiguration is a typical MINLP model with the objective function of minimizing the operation complexity index, given by Eq. (12) and various constraints given by Eqs. (13)–(31).

$$\min f = \sum_{(i,j,c) \in L_{\text{un}}} z_{ijc} + k_1 \left( \sum_{(i,j,c) \in L} z_{ijc} - \sum_{i \in N} m_i + 1 \right) + k_2 \sum_{(i,j,c) \in L_{\text{un}}} z_{ijc} \frac{b_{ijc}}{b_{\text{base}}} \quad (12)$$

##### (1) Node power balance constraint sets

$$\sum_{(i,j,c) \in L^{\text{to}}} P_{ijc,t}^s - \sum_{(i,j,c) \in L^{\text{from}}} P_{ijc,t}^s + \sum_{g \in G} P_{g,t}^s + \sum_{w \in W} P_{w,t}^{\text{pre}} = P_{di,t} \quad (13)$$

$$\forall i \in N, t \in T, s \in S$$

$$\sum_{(i,j,c) \in L^{\text{to}}} Q_{ijc,t}^s - \sum_{(i,j,c) \in L^{\text{from}}} Q_{ijc,t}^s + \sum_{g \in G} Q_{g,t}^s = Q_{di,t} \quad (14)$$

$$\forall i \in N, t \in T, s \in S$$

##### (2) AC power flow constraint sets

$$P_{ijc,t}^s = z_{ijc} \left[ -v_{i,t}^s v_{j,t}^s \left( g_{ijc} \cos \theta_{ij,t}^s + b_{ijc} \sin \theta_{ij,t}^s \right) + g_{ijc} \left( v_{i,t}^s \right)^2 \right] \quad (15)$$

$$\forall (i,j,c) \in L, t \in T, s \in S$$

$$Q_{ijc,t}^s = z_{ijc} \left[ v_{i,t}^s v_{j,t}^s \left( b_{ijc} \cos \theta_{ij,t}^s - g_{ijc} \sin \theta_{ij,t}^s \right) - b_{ijc} \left( v_{i,t}^s \right)^2 \right] \quad (16)$$

$$\forall (i,j,c) \in L, t \in T, s \in S$$

##### (3) Power flow transmission constraint sets

$$P_{ijc}^{\min} z_{ijc} \leq P_{ijc,t}^s \leq P_{ijc}^{\max} z_{ijc} \quad \forall (i,j,c) \in L, t \in T, s \in S \quad (17)$$

$$Q_{ijc}^{\min} z_{ijc} \leq Q_{ijc,t}^s \leq Q_{ijc}^{\max} z_{ijc} \quad \forall (i,j,c) \in L, t \in T, s \in S \quad (18)$$

##### (4) Unit output constraint sets

$$P_g^{\min} \leq P_{g,t}^s \leq P_g^{\max} \quad \forall g \in G_{\text{BS}}, t \in T, s \in S \quad (19)$$

$$P_{g,t}^s = P_g^{\text{fixed}} \quad \forall g \in (G - G_{\text{BS}}), t \in T, s \in S \quad (20)$$

$$Q_g^{\min} \leq Q_{g,t}^s \leq Q_g^{\max} \quad \forall g \in G_{\text{BS}}, t \in T, s \in S \quad (21)$$

$$Q_{g,t}^s = 0 \quad \forall g \in (G - G_{\text{BS}}), t \in T, s \in S \quad (22)$$

##### (5) Voltage and phase angle constraint sets

$$v_i^{\min} \leq v_{i,t}^s \leq v_i^{\max} \quad \forall i \in N, t \in T, s \in S \quad (23)$$

$$\theta_i^{\min} \leq \theta_{i,t}^s \leq \theta_i^{\max} \quad \forall i \in N, t \in T, s \in S \quad (24)$$

##### (6) Wind power output constraint set

$$P_{w,t}^{\min} \leq P_{w,t}^{\text{pre}} \leq P_{w,t}^{\max} \quad \forall w \in W, t \in T, s \in S \quad (25)$$

##### (7) Control variable constraint sets

$$z_{ijc} = 1 \quad \forall (i,j,c) \in L_{\text{en}} \quad (26)$$

$$\sum_{(i,j,c) \in L_{\text{un}}} z_{ijc} \leq J \quad (27)$$

##### (8) Corresponding constraint sets of lines and nodes

$$m_i \leq M \left( \sum_{j \in (i,j,c)} z_{ijc} + \sum_{j \in (j,i,c)} z_{jic} \right) \quad \forall i, j \in N, (i,j,c)/(j,i,c) \in L \quad (28)$$

$$m_i \geq \frac{1}{M} \left( \sum_{j \in (i,j,c)} z_{ijc} + \sum_{j \in (j,i,c)} z_{jic} \right) \quad \forall i, j \in N, (i,j,c)/(j,i,c) \in L \quad (29)$$

$$m_i \in \{0, 1\} \quad \forall i \in N \quad (30)$$

##### (9) SPA constraint set

$$\theta_{ij,t}^s \leq \theta_{\text{set}} \quad \forall (i,j) \in L_{\text{en}} \quad (31)$$

In the above constraints, Eqs. (28)–(30) are the analytic mapping constraint sets for the restored nodes and restored lines through the large  $M$  relaxation method. Only when all the lines connected to node  $i$  are not put into operation, node  $i$  is in uncharged state. Besides, Eqs. (13)–(14) and Eqs. (17)–(30) can be included in a linear programming model. However, Eqs. (15)–(16) and Eq. (31) are difficult to be linearized. Therefore, this paper proposes a two-layer solving framework by using a separate model to check the SPA constraint and AC power flow constraints, as given in Section 5.

## 5. Solving of loop-network reconfiguration optimization model

The MINLP model considering AC power flow constraints and the SPA constraint is difficult to solve, and the solution optimality cannot be guaranteed. Therefore, we consider to replace AC power flow constraints with DC power flow constraints to transform the MINLP model into a MILP model for fast solving. However, the node voltage amplitude and reactive power distribution cannot be obtained by the DC power flow model. Meanwhile, the SPA constraint for loop-closing operation cannot be checked by the DC power flow model. In view of this, a two-layer solving framework is proposed to simplify the solving of the loop-network optimization model. In the upper-level layer, the loop-network reconfiguration scheme is solved by an MILP model considering DC power flow constraints. In the lower-level layer, the optimal scheme given by the MILP model is checked by AC power flow constraints and SPA constraint. An alternative and iterative solving process is then employed to get the optimal scheme. If no constraint is violated after calculation of the AC power flow in the iteration process, the iteration is

terminated and the optimal loop-network reconfiguration scheme is acquired. Otherwise, the infeasible optimal scheme is removed from the solution space by adding an infeasible cut constraint, and a new iteration is carried out until a feasible scheme is obtained.

### 5.1. MILP model considering DC power flow constraints

The objective function of the loop-network reconfiguration MILP model is given by Eq. (32).

$$\min f = \sum_{(i,j,c) \in L_{un}} z_{ijc} + k_1 \left( \sum_{(i,j,c) \in L} z_{ijc} - \sum_{i \in N} m_i + 1 \right) + k_2 \sum_{(i,j,c) \in L_{un}} z_{ijc} \frac{b_{ijc}}{b_{base}} \quad (32)$$

The constraints are given by Eqs. (33)–(45).

#### 1) Node active power balance constraint set

$$\sum_{(i,j,c) \in L^{to}} P_{ijc,t}^s - \sum_{(i,j,c) \in L^{from}} P_{ijc,t}^s + \sum_{g \in G} P_{g,t}^s + \sum_{w \in W} P_{w,t}^{pre} = P_{di,t} \quad (33)$$

$$\forall i \in N, t \in T, s \in S$$

#### 2) DC power flow constraint sets

$$\frac{1}{x_{ijc}} \left( \theta_{i,t}^s - \theta_{j,t}^s \right) - P_{ijc,t}^s + (1 - z_{ijc}) M \geq 0 \quad (34)$$

$$\forall (i,j,c) \in L, t \in T, s \in S$$

$$\frac{1}{x_{ijc}} \left( \theta_{i,t}^s - \theta_{j,t}^s \right) - P_{ijc,t}^s - (1 - z_{ijc}) M \leq 0 \quad (35)$$

$$\forall (i,j,c) \in L, t \in T, s \in S$$

#### 3) Active power flow transmission constraint set

$$P_{ijc}^{min} z_{ijc} \leq P_{ijc,t}^s \leq P_{ijc}^{max} z_{ijc} \quad \forall (i,j,c) \in L, t \in T, s \in S \quad (36)$$

#### 4) Active power output constraint sets of units

$$P_g^{min} \leq P_{g,t}^s \leq P_g^{max} \quad \forall g \in G_{BS}, t \in T, s \in S \quad (37)$$

$$P_{g,t}^s = P_g^{fixed} \quad \forall g \in (G - G_{BS}), t \in T, s \in S \quad (38)$$

#### 5) Node phase angle constraint set

$$\theta_i^{min} \leq \theta_{i,t}^s \leq \theta_i^{max} \quad \forall i \in N, t \in T, s \in S \quad (39)$$

#### 6) Wind power output constraint set

$$P_{w,t}^{min} \leq P_{w,t}^{pre} \leq P_{w,t}^{max} \quad \forall w \in W, t \in T, s \in S \quad (40)$$

#### 7) Control variable constraint sets

$$z_{ijc} = 1 \quad \forall (i,j,c) \in L_{en} \quad (41)$$

$$\sum_{(i,j,c) \in L_{un}} z_{ijc} \leq J \quad (42)$$

#### 8) Corresponding constraint sets of lines and nodes

$$m_i \leq M \left( \sum_{j \in (i,j,c)} z_{ijc} + \sum_{j \in (j,i,c)} z_{ijc} \right) \quad \forall i, j \in N, (i,j,c)/(j,i,c) \in L \quad (43)$$

$$m_i \geq \frac{1}{M} \left( \sum_{j \in (i,j,c)} z_{ijc} + \sum_{j \in (j,i,c)} z_{ijc} \right) \quad \forall i, j \in N, (i,j,c)/(j,i,c) \in L \quad (44)$$

$$m_i \in \{0, 1\} \quad \forall i \in N \quad (45)$$

### 5.2. Verification of SPA constraint and AC power flow constraints

The loop-closing operation cannot be executed if the phase angles of the to-be-restored nodes does not meet the SPA constraint. Likewise, at network reconfiguration stage, the breakthrough of the node voltage limit will seriously threaten the security of the power system. Therefore, the voltage and phase of the recovered nodes must be considered in network reconfiguration, and AC power flow calculation is required.

#### a) Verification of AC power flow constraints

The AC power flow constraints are shown in the following Eqs. (46)–(49).

##### 1) AC power flow constraint sets for lines

$$P_{ijc,t}^s = \widehat{z}_{ijc} \times \left[ -v_{i,t}^s v_{j,t}^s \left( g_{ijc} \cos \theta_{ij,t}^s + b_{ijc} \sin \theta_{ij,t}^s \right) + g_{ijc} \left( v_{i,t}^s \right)^2 \right] \quad (46)$$

$$\forall (i,j,c) \in L, i \in N, t \in T, s \in S$$

$$Q_{ijc,t}^s = \widehat{z}_{ijc} \times \left[ v_{i,t}^s v_{j,t}^s \left( b_{ijc} \cos \theta_{ij,t}^s - g_{ijc} \sin \theta_{ij,t}^s \right) - b_{ijc} \left( v_{i,t}^s \right)^2 \right] \quad (47)$$

$$\forall (i,j,c) \in L, i \in N, t \in T, s \in S$$

##### 2) Transfer power limit constraint sets for lines

$$P_{ijc}^{min} \widehat{z}_{ijc} \leq P_{ijc,t}^s \leq P_{ijc}^{max} \widehat{z}_{ijc} \quad \forall (i,j,c) \in L, t \in T, s \in S \quad (48)$$

$$Q_{ijc}^{min} \widehat{z}_{ijc} \leq Q_{ijc,t}^s \leq Q_{ijc}^{max} \widehat{z}_{ijc} \quad \forall (i,j,c) \in L, t \in T, s \in S \quad (49)$$

The verification of AC power flow constraints is a typical NLP problem, and we use the KNITRO solver in GAMS to solve it. If the verification of AC power flow constraints passes, the SPA constraint verification is then carried out. Otherwise, the constraint verification ends and the reconfiguration scheme is labeled “infeasible”. Next, a linear constraint of the infeasible cut is added directly to the upper model, and a new iteration starts. This process is repeated until AC power flow constraints and SPA constraint are both met. The infeasible cut linear constraint is described by Eq. (50).

$$\sum_{(i,j,c) \in (L_{un} - E_l)} z_{ijc} \geq 1, \quad \forall E_l \subseteq K_l \quad (50)$$

Through Eq. (50), the infeasible schemes are continuously deleted from the optimization domain and the optimization process repeats again, until they satisfy SPA constraint and AC power flow constraints. The most important common feature of the infeasible schemes is that they all contain all the lines of the optimal scheme. Besides, the elements of  $E_l$  for each iteration change according to its condition, and all infeasible schemes can be eliminated. Therefore, the infeasible cut constraint is of significance for obtaining the optimal scheme satisfying the requirements.

#### b) Verification of SPA constraint

The phase angles of the recovered nodes are related to the active power distribution of the power system. Therefore, the phase angle of a recovered node is considered to be constant before a line charge and after. The phase angles of the nodes before the line charging are used to verify SPA constraint given by Eq. (51).

$$-\theta_{set} \leq \theta_i^s - \theta_j^s \leq \theta_{set} \quad \forall i, j \in N_{re}^s \quad (51)$$

The SPA constraints cannot be used directly in the main body of the optimization process. It needs to be implemented by the classic graph

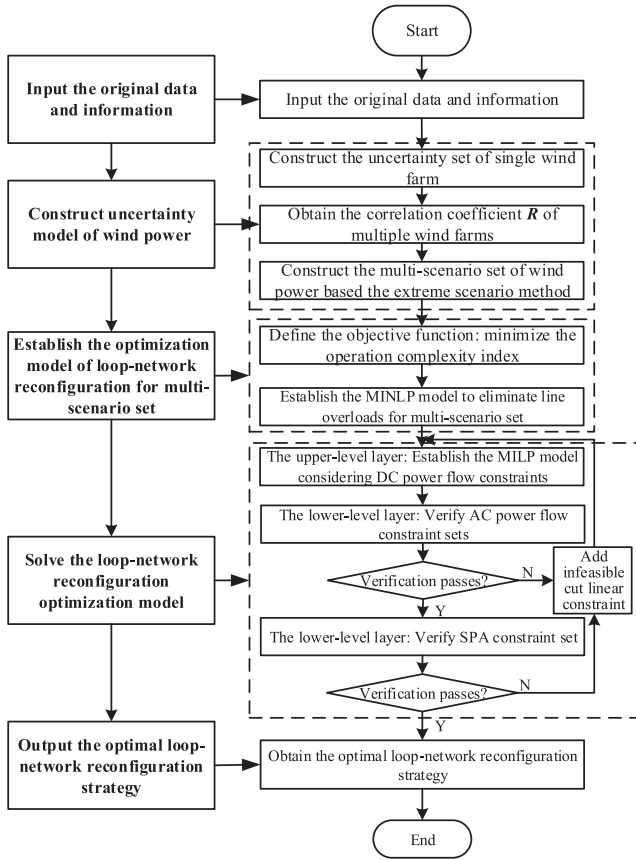


Fig. 3. Flow chart of loop-network reconfiguration optimization.

theory algorithm in computer science. The specific verification process is as follows.

1) The matrix  $A_{N \times N}^s$  is defined as follows. For the to-be-restored node  $i$  and the node  $j$  in the  $s$ th scenario, if  $\theta_i^s - \theta_j^s > \theta_{set}$ ,  $A_{ij}^s = 1$ ; if  $\theta_i^s - \theta_j^s < \theta_{set}$ ,  $A_{ij}^s = 0$ . In addition, if  $i$  or  $j$  has not been recovered before the network adjustment,  $A_{ij}^s = 0$ .

2) In the  $l$ th iteration of the  $s$ th scenario, define the adjacency matrix of to-be-restored lines determined by the upper-level layer to be  $I_{N \times N}^{s,l}$ . In addition, the node  $i$  and node  $j$  are directly connected, then  $F_{ij}^{s,l} = 1$ ; otherwise, it is 0. The reachability matrix  $C_{N \times N}^{s,l}$  is defined as follows. In network topology with all the to-be-restored lines which is determined by the upper-level layer, if there is a path from the node  $i$  to the node  $j$ , then  $C_{ij} = 1$ ; otherwise, it is 0. The reachability matrix  $C_{N \times N}^{s,l}$  can be obtained from the adjacency matrix  $I_{N \times N}^{s,l}$  by the Floyd-Warshall algorithm.

Further, an intermediate variable matrix  $A_{temp}^{s,l}$  is defined by Eq. (52).

$$A_{temp}^{s,l} = A \circ C^{s,l} \quad (52)$$

where, “ $\circ$ ” is the Hadamard product of two same-order matrices. The following conclusions can be drawn by applying  $A_{ij,temp}^{s,l} = A_{ij}^{s,l} \times C_{ij}^{s,l}$ .

$$N_{\theta, infeas}^{s,l} = \sum A_{ij,temp}^{s,l} \quad (53)$$

In Eq. (53), if  $N_{\theta, infeas}^{s,l}$  is 0, the SPA constraint of the scheme is verified. Otherwise, the verification fails and it returns to the main model program with the infeasible cut linear constraint as given by Eq. (50).

Therefore, the flow chart of loop-network reconfiguration optimization to eliminate line overloads with large-scale wind power integration is shown in Fig. 3.

## 6. Case study

The IEEE 39-bus system and the IEEE 118-bus system were modified and taken as instances to verify effectiveness of the proposed loop-network reconfiguration optimization model. The relevant parameters were set as follows:  $\theta_{set} = 18^\circ$ ,  $k_1 = 5$ ,  $k_2 = 0.001$ ,  $J_1 = 6$ ,  $J_2 = 15$  and  $T = 30$  min. In the time period  $T$ , it was assumed that the status and amount of the restored loads remain unchanged. GAMS was employed to model and solve the optimization problem. The CPLEX solver (set to four threads) was used to solve the MILP model and the KNITRO solver to solve the NLP model. The computation platform was a PC with Intel (R) Core (TM) i5-4210U CPU and the installed memory 4 GB.

### 6.1. Case study I: Modified IEEE 39-bus power system

The IEEE 39-bus power system was modified by integrating two wind farms on nodes 16 and 18 and it was taken as Case study I, shown in Fig. 4. In the current restoration state, unit 30 was used as the black-start unit and the units on the buses 35, 37, and 38 had been restarted successfully. The restored lines were represented by the solid black lines in Fig. 4. Two wind farms were at the receiving end of the currently restored network. Meanwhile, the restored line 26–27 encountered overloading risk, so a loop-network reconfiguration scheme was required. The proposed method was employed to obtain the optimal loop-network reconfiguration scheme. The operational data of the two wind farms referred to the data of wind farms in Inner Mongolia of China.

The predicted wind power outputs obeyed the Gauss distribution, and the spatiotemporal correlation coefficient matrix of the two wind

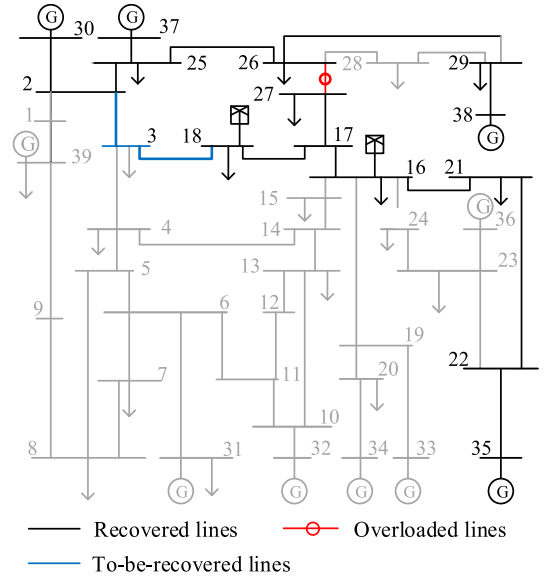


Fig. 4. Schematic of the loop-network reconfiguration scheme for Case study I.

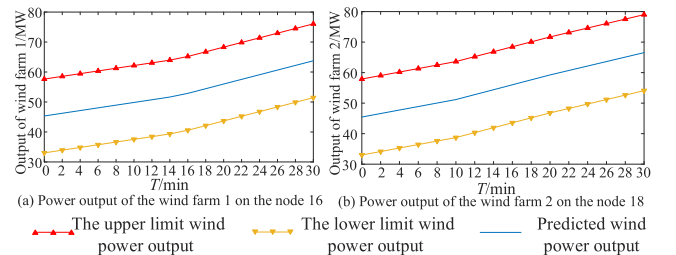


Fig. 5. Schematics of the upper and lower output limits of two wind farms.

**Table 1**  
Optimal loop-network reconfiguration scheme.

Lines selected	New lines charging reactive power/Mvar	Power flow before adjustment/MW	Power flow after adjustment/MW	Number of loop-network
2-3 3-18	48.0	677.2	412.4	1

farms is given by Eq. (54). The output upper and lower limits of the two wind farms based on the extreme scenario method are demonstrated in Fig. 5, where the confidence level  $\alpha$  was set to 15%.

$$R = \begin{bmatrix} 1 & 0.9954 \\ 0.9954 & 1 \end{bmatrix} \quad (54)$$

When two wind farms are connected to the system, there are four extreme scenarios, requiring a multi-scenario set including all extreme scenarios. However, these two wind farms were located at the receiving end, so the worst scenario was formed by the lowest wind power outputs and only the lowest wind power output needed to be considered. The outputs of wind farm 1 and wind farm 2 were 33.029 MW and 33.005 MW respectively.

Here, the line 26–27 was overloaded (exceeding the transfer limit of 600 MW). Then the loop-network reconfiguration scheme was required to eliminate line 26–27 overload. The scheme obtained by the upper-level layer model just passed the lower-level layer verification including AC power flow constraints and SPA constraint, so the final optimal scheme is obtained without iteration, as given in Table 1. The transmission lines selected to form the loop-network are shown in Fig. 4, the solid blue lines.

6.2. Case study II: Modified IEEE 118-bus system

The IEEE118-bus system was modified to further verify effectiveness

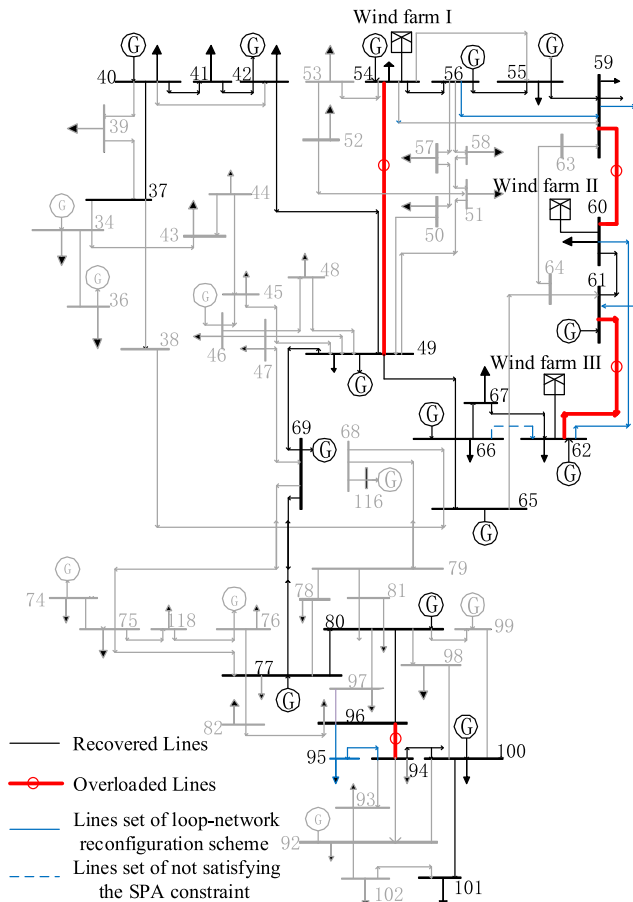


**Fig. 6.** Schematic of the loop-network reconfiguration scheme for Case study II.

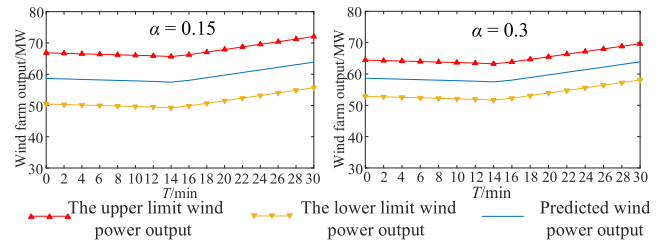


**Fig. 7.** Schematics of the wind farm outputs when  $\alpha = 0.15$  and  $\alpha = 0.3$ .

of the proposed method, taken as Case study II and shown in Fig. 6. The unit on node 69 was used as the black-start unit, and some units, loads and lines had been restored to form the network structure, represented by the black solid lines in Fig. 6. The units' recovery states are given in Appendix A1. For the power transfer limits of the lines were not mentioned in the original data of the IEEE118-bus system [38], the transfer limits of lines were hypothetical (See Appendix A2 for detail).

Different from Case study I, with wind farms connected to the system, for the case that the sending-end and the receiving end cannot be recognized distinctly, the worst scenario cannot be easily concluded from the expected wind power outputs. Therefore, a multi-scenario set of the wind power outputs was required, and the optimal loop-network reconfiguration scheme needed to satisfy the multi-scenario set simultaneously.

Different values of the confidence level  $\alpha$  decided the number of the error scenarios. Fig. 7 is a schematic of the power outputs of a wind farm

**Table 2**  
Descriptive information for each scenario.

Scenarios description	Wind farm output		
	$P_{w1}/MW$	$P_{w2}/MW$	$P_{w3}/MW$
Scenario I	33.029	49.275	33.005
Scenario II	33.029	72.055	33.005
Scenario III	33.029	49.275	79.007
Scenario IV	33.029	72.055	79.007
Scenario V	76.071	49.275	33.005
Scenario VI	76.071	72.055	33.005
Scenario VII	76.071	49.275	79.007
Scenario VIII	76.071	72.055	79.007

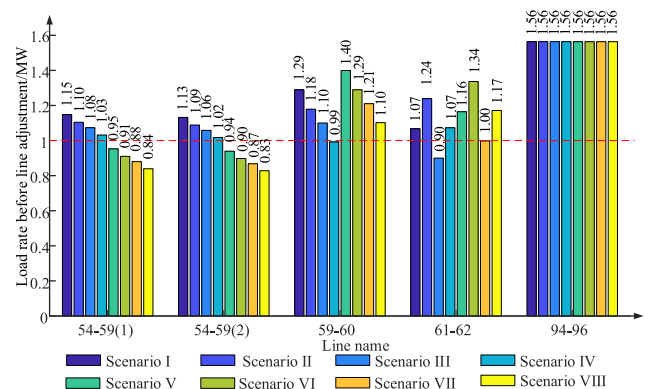


**Fig. 8.** Loading ratio before loop-network operation.

**Table 3**

Active power flow before loop-network reconfiguration operation in each scenario (MW).

Scenario	Line	Line	Line	Line
	49–54	59–60	61–62	94–96
Scenario I	126.32/124.53	103.12	90.73	156.37
Scenario II	121.49/119.77	94.33	105.35	156.37
Scenario III	118.07/116.40	88.00	76.52	156.37
Scenario IV	113.49/111.90	79.37	91.22	156.37
Scenario V	104.81/103.36	111.96	98.97	156.37
Scenario VI	100.11/98.74	103.17	113.63	156.37
Scenario VII	96.78/95.47	96.83	84.84	156.37
Scenario VIII	92.31/91.09	88.19	99.58	156.37

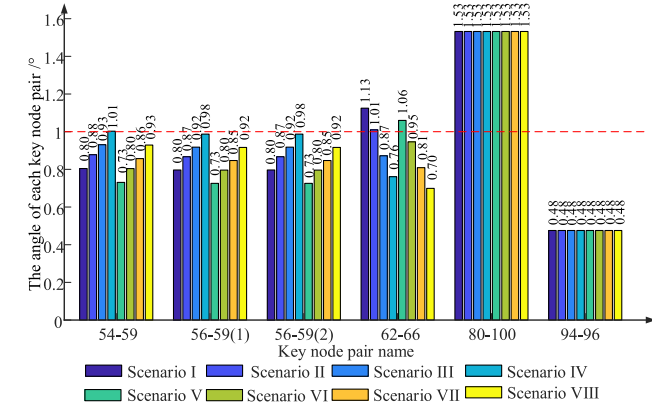


**Fig. 9.** The angle of each key node pair in different scenarios.

when  $\alpha$  was 0.15 and 0.3. It can be clearly seen that when  $\alpha$  was 0.15, it included more error scenarios. Therefore, the confidence level  $\alpha$  was set to 0.15 in this paper.

As shown in Fig. 6, three wind farms participated in the loop-network reconfiguration. For better illustration, the wind farm 1 and farm 2 used in Case study I were defined as wind farm I and wind farm III and were connected to nodes 54 and 62 respectively. Meanwhile, a wind farm

**Table 4**

Information of iteration results.

Iterations	Line sets	Feasibility
1	56–59(1) 62–66 94–95 95–96	No, the node pairs 62–66 cannot satisfy the SPA constraint
2	54–59 62–66 94–95 95–96	No, the node pairs 54–59 cannot satisfy the SPA constraint
3	56–59(2) 62–66 80–98 98–100	No, the node pair 62–66 and 80–100 cannot satisfy the SPA constraint
4	56–59(2) 62–66 80–99 99–100	
5	56–59(1) 62–66 80–99 99–100	
6	56–59(1) 62–66 80–98 98–100	
7	54–59 62–66 80–99 99–100	No, the node pairs 54–59, 62–66 and 80–100 cannot satisfy the SPA constraint
8	54–59 62–66 80–98 98–100	
9	56–59(2) 59–61 60–62 94–95 95–96	Yes

**Table 5**

Loop-network reconfiguration strategy for eliminating line overloads.

Scenario	The optimal scheme	charging reactive power/Mvar	Power flow after lines adjustment/MW			
			Line 49–54	Line 59–60	Line 61–62	Line 94–96
Scenario I	56–59(2) 59–61	13	109.0/ 108.3	56.0	71.7	86.4
Scenario II	60–62 94–95		99.4/ 98.7	46.3	60.5	86.4
Scenario III	95–96		103.8/ 103.1	50.3	77.6	86.4
Scenario IV			94.2/ 93.5	40.6	66.4	86.4
Scenario V			92.4/ 91.7	61.0	77.5	86.4
Scenario VI			82.7/ 82.1	51.3	66.2	86.4
Scenario VII			87.2/ 86.6	55.3	83.4	86.4
Scenario VIII			77.5/ 77.0	45.6	72.2	86.4

with power outputs shown by Fig. 7 was connected to node 60, named as wind farm II. The operational data of the wind farm II also referred to the data of wind farms in Inner Mongolia and the correlation coefficient matrix of three wind farms was given by Eq. (55). Obviously, when the number of wind farms was three, the number of extreme scenarios in the multi-scenario set here was eight and the descriptive information for each scenario was given in Table 2.

$$R = \begin{bmatrix} 1 & 0.8857 & 0.9954 \\ 0.8857 & 1 & 0.8410 \\ 0.9954 & 0.8410 & 1 \end{bmatrix} \quad (55)$$

When the wind farms participated in loop-network reconfiguration, the risk of line overload was aggravated. Fig. 8 was the loading ratios before loop-network reconfiguration operation in eight scenarios and the power output values (MW) were shown in Table 3. It was clearly that the double-circuit line 49–54, line 59–60, line 61–62 and line 94–96 were overloaded, as shown in Fig. 8. The settings of transfer limits were 110 MW, 80 MW, 85 MW and 100 MW respectively. Therefore, it is necessary to eliminate the line overloads by the proposed model.

In the upper-level layer model, the optimal line set for loop-network reconfiguration scheme included line 56–59 (2), line 62–66, line 94–95, and line 95–96, represented by the blue dotted lines in Fig. 6. Then in the lower-level layer checking, it needed to check the SPA of each key node pair. If the angle of lines obtained from the upper-level layer model did not meet the SPA constraint, the next iterative calculation needed to be

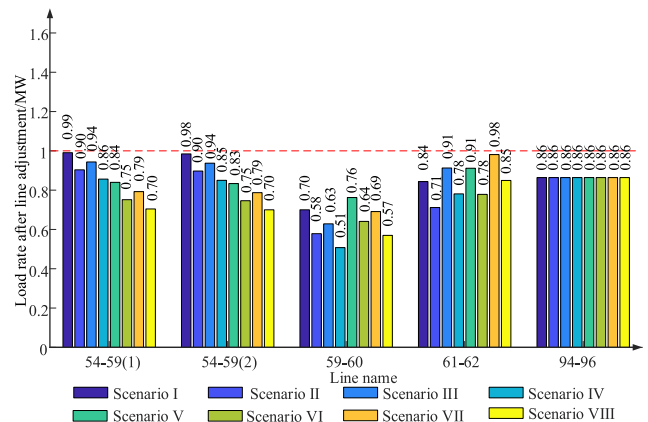


**Fig. 10.** Schematic of line loading ratios after loop-network reconfiguration.

carried out until a feasible optimal solution is obtained. Fig. 9 is the angle of each key node pair in different scenarios. It is clearly that the node pair 54–59, node pair 62–66 and node pair 80–100 cannot satisfy SPA constraint in eight scenarios simultaneously, so the optimal loop-network strategy was determined through eight iterations, as shown in Table 4.

The loop-network reconfiguration optimization model with DC power flow constraints was a typical MILP problem, and it can ensure optimality and high computational efficiency based on the CPLEX solver. By adding the infeasible cut linear constraint, the infeasible schemes were prohibited, and the solving process was guided to a feasible optimal scheme with verification of SPA constraint and AC power flow constraints. Thus, the optimal loop-network reconfiguration strategy satisfying all the constraints for multi-scenario set was obtained, as listed in Table 5 and shown in blue solid lines in Fig. 6. To depict it more directly, we gave the line loading ratios after the loop-network reconfiguration, as shown in Fig. 10. It could be seen that through the loop-network reconfiguration, the line overloads were eliminated, which demonstrates effectiveness of the proposed optimization method.

### 6.3. Case study III: Yunnan power system in southwest China

To illustrate effectiveness of the proposed model, the test was carried out on the Yunnan power system in China. The system included 194 stations, 55 generating plants, 486 transmission lines with the voltages of 220 kV and above. For better illustration, only 500 kV power stations and part of 220 kV power stations were shown in Fig. 11. The black-start unit was XW and the units of ZX, MW, KM, QJD and XLT had been successfully restarted. The restored lines are in solid black lines in Fig. 11. Three wind farms named HPF, YFF, QJF, were connected to the nodes of HP, YF and QJ respectively. Due to the uncertainty of wind power output or the large amount of load restoration which makes some

units out of operation, three lines named line HP-QJ, line CP-BF, line BF-YX, were overloaded in the system.

After solving and verifying the model, the optimal scheme was obtained, and it satisfied SPA constraint and AC power flow constraints, as shown by the solid green lines in Fig. 11. In the optimal scheme, the line overloads were eliminated by restoring five additional lines, namely line SC-CP, line BF-QD, line QD-LP, line QD-QS, line MJ-HL, to construct loop-network in the restored area. Besides, the power carrying capacity and handling ability to wind power fluctuations of the network structure were also improved significantly. The optimization result demonstrates effectiveness of the proposed method in this paper, and shows its applicability for the elimination of line overloads in the actual provincial transmission network reconfiguration, especially in the case with wind power integration.

## 7. Conclusions

An optimization method of loop-network reconfiguration considering large-scale wind power integration is proposed to eliminate line overloads in the black-start process. A MINLP model of loop-network reconfiguration considering the multi-scenario set simultaneously is established. A two-layer solving framework is proposed to solve the optimization model. The optimal loop-network restoration scheme is obtained by means of a hierarchical iterative solving process. The proposed method is verified by the numerical results of two IEEE standard power system cases and an actual provincial power system case. The proposed method can be used by the power system operators to make more secure restoration schemes.

The future work is planned as follows: 1) Corresponding efficient calculation strategies will be studied further to shorten calculation time of loop-network reconfiguration model; 2) The load uncertainty will be considered in long term restoration process after a major blackout.

### CRedit authorship contribution statement

**Shaoyan Li:** Writing - review & editing, Supervision. **Liyuan Wang:** Conceptualization, Methodology, Software, Writing – original draft. **Xueping Gu:** Writing - review & editing, Supervision. **Hanguang Zhao:** Writing - review & editing, Supervision. **Yongzhao Sun:** Writing - review & editing, Supervision.

### Declaration of Competing Interest

The authors declare that they have no known competing financial interests or personal relationships that could have appeared to influence the work reported in this paper.

### Acknowledgement

This work was supported by National Natural Science Foundation of China (Project No. 52107092), Natural Science Foundation of Hebei Province (Project No. E2019502195) and the Fundamental Research Funds for the Central Universities (Project No.2021MS063).

### Appendix A1

Appendix A1 is about the recovery status of units in scene I to scene VIII, given in Table A1.

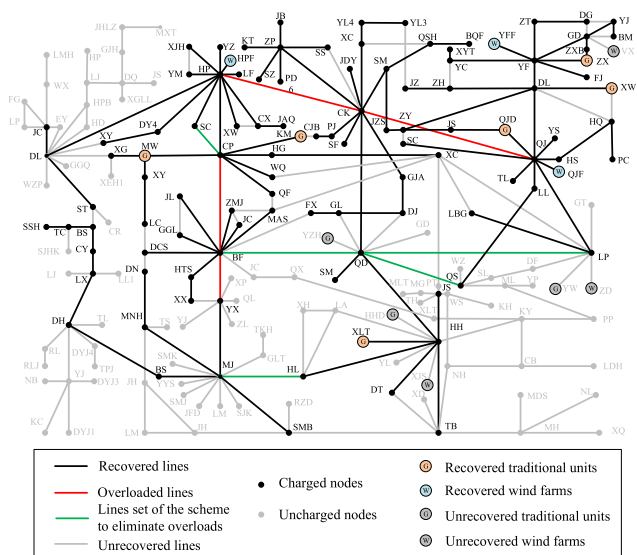


Fig. 11. Initial state of Yunnan power system and the final scheme to eliminate line overloads.

**Table A1**

The restoration status of generator units in Scene I to Scene VIII.

Scene		40	42	49	54	55	56	59	61	62	65	66	69	77	80	100
Scene I	Active power/MW	50.0	0.0	304.0	140.0	50.0	20.0	205.0	200.0	20.0	51.0	292.0	-149.1	0.0	477.0	252.0
	Reactive power/Mvar	35.9	27.0	12.8	102.4	-1.1	42.3	-16.6	6.7	81.5	72.7	2.3	86.5	27.4	90.1	44.6
Scene II	Active power/MW	50.0	30.0	304.0	140.0	50.0	20.0	205.0	200.0	20.0	51.0	292.0	-175.0	0.0	477.0	252.0
	Reactive power/Mvar	35.9	27.0	8.3	99.0	0.4	42.8	-16.3	1.3	76.6	72.7	-2.4	94.6	27.4	90.1	44.6
Scene III	Active power/MW	50.0	30.0	304.0	140.0	50.0	20.0	205.0	200.0	20.0	51.0	292.0	-200.0	0.0	477.0	252.0
	Reactive power/Mvar	35.9	27.0	7.4	96.7	1.7	43.1	-15.3	4.4	59.7	72.7	7.0	104.9	27.4	90.1	44.6
Scene IV	Active power/MW	50.0	30.0	304.0	140.0	50.0	20.0	205.0	200.0	20.0	51.0	292.0	-222.4	0.0	477.0	252.0
	Reactive power/Mvar	35.9	27.0	8.0	93.69	3.5	43.5	-14.5	-1.0	56.2	72.7	-10.0	116.3	27.4	90.1	44.6
Scene V	Active power/MW	50.0	30.0	304.0	140.0	50.0	20.0	205.0	200.0	20.0	51.0	292.0	-199.6	0.0	477.0	252.0
	Reactive power/Mvar	35.9	27.0	-0.9	75.8	-2.4	41.9	-17.0	8.3	78.7	72.7	-0.8	104.6	27.4	90.1	44.6
Scene VI	Active power/MW	50.0	30.0	304.0	140.0	50.0	20.0	205.0	200.0	20.0	51.0	292.0	-222.5	0.0	477.0	252.0
	Reactive power/Mvar	35.9	27.0	-0.1	73.1	-1.1	42.3	-17.0	2.8	74.2	72.7	-4.7	116.3	27.4	90.1	44.6
Scene VII	Active power/MW	50.0	30.0	304.0	140.0	50.0	20.0	205.0	200.0	20.0	51.0	292.0	-244.8	0.0	477.0	252.0
	Reactive power/Mvar	35.9	27.0	4.0	71.3	-0.0	42.6	-16.2	5.7	57.6	72.7	-8.8	130.1	27.4	90.1	44.6
Scene VIII	Active power/MW	50.0	30.0	304.0	140.0	50.0	20.0	205.0	200.0	20.0	51.0	292.0	-264.5	0.0	477.0	252.0
	Reactive power/Mvar	35.9	27.0	9.4	68.9	1.6	43.1	-15.7	0.3	54.5	72.7	-11.3	144.7	27.4	90.1	44.6

**Appendix A2**

Appendix A2 is about the assuming transfer limit of each line, given in Table A2.

**Table A2**

The assuming transfer limit of each line.

Lines	Transfer limit of lines/MW	Lines	Transfer limit of lines/MW	Lines	Transfer limit of lines/MW
37-40	100	40-41	100	41-42	100
42-49	200	49-54(1)	110	49-54(2)	110
49-66(1)	100	49-66(2)	100	49-69	200
54-56	60	55-56	100	55-59	100
56-59(2)	100	59-60	80	59-61	80
60-61	200	60-62	60	61-62	85
62-67	200	65-66	100	66-67	200
69-77	250	77-80(1)	400	77-80(2)	400
80-96	200	94-95	100	94-96	100
94-100	300	95-96	100	100-101	100

**References**

- Zheng Y, Dong ZY, Meng K, et al. Multi-objective distributed wind generation planning in an unbalanced distribution system. *CSEE J Power Energy Syst* 2017;3(2):186-95.
- Erdiwansyah, Mahidin, Husin H, et al. A critical review of the integration of renewable energy sources with various technologies. *Protect Control Modern Power Syst* 2021;6(1):37-54.
- Fink LH, Liou KL, Liu CC. From generic restoration actions to specific restoration strategies power system restoration dynamics issues. *IEEE Trans Power Syst* May 1995;10(2):745-52.
- Liu L, Wu J, Mi Z, et al. A feasibility study of applying storage-based wind farm as black-start power source in local power grid. In: 2016 International Conference on Smart Grid and Clean Energy Technologies (ICSGCE), Chengdu; 2016. p. 257-61.
- Golshani A, Sun W, Zhou Q, et al. Incorporating Wind Energy in Power System Restoration Planning. *IEEE Trans Smart Grid* 2019;10(1):16-28.
- Zhao J, Wang H, Liu Y, et al. Utility-Oriented Online Load Restoration Considering Wind Power Penetration. *IEEE Trans Sustain Energy* 2019;10(2):706-17.
- Zhao J, Wang H, Wu Q, et al. Distributed Risk-Limiting Load Restoration for Wind Power Penetrated Bulk System. *IEEE Trans Power Syst* Sept. 2020;35(5):3516-28.
- Li S, Gu X, Zhou G, Li Y. Optimisation and comprehensive evaluation of alternative energising paths for power system restoration. *IET Gener Transm Distrib* May 2019;13(10):1923-32.
- Xie Y, Li D, Xu Y, et al. A MILP-based restoration planning method for generator start-up considering flexible re-energizing times of transmission lines. *Int J Electrical Power Energy Syst* 2021;124. <https://doi.org/10.1016/j.ijepes.2020.106357>.
- Liu Y, Gu X. Skeleton-Network reconfiguration based on topological characteristics of scale-free Networks and discrete particle swarm optimization. *IEEE Trans Power Syst* Aug. 2007;22(3):1267-74.
- Sun W, Liu C-C, Zhang L. Optimal generator start-up strategy for bulk power system restoration. *IEEE Trans Power Syst* Aug. 2011;26(3):1357-66.
- Gu X, Liu W, Sun C. Optimisation for unit restarting sequence considering decreasing trend of unit start-up efficiency after a power system blackout. *IET Gener Transm Distrib* Dec. 2016;10(16):4187-96.
- Gu X, Zhou G, Li S, et al. Global optimisation model and algorithm for unit restarting sequence considering black-start zone partitioning. *IET Gener Transm Distrib* Jul. 2019;13(13):2652-63.
- Sun L, Lin Z, Xu Y, et al. Optimal skeleton-network restoration considering generator start-up sequence and load pickup. *IEEE Trans Smart Grid* May 2019;10(3):3174-85.
- Merlin A, Desbrosses JP. European incident of 4th November 2006-the events and the first lessons drawn. *Electra* 2007;230:4-11.
- Schnyder G, Glavitsch H. Integrated security control using an optimal power flow and switching concepts. *IEEE Trans Power Syst* May 1988;3(2):782-90.
- Makram EB, Thorton KP, Brown HE. Selection of lines to be switched to eliminate overloaded lines using a Z-matrix method. *IEEE Trans Power Syst* May 1989;4(2):653-61.
- Bakirtzis AG, Meliopoulos APS. Incorporation of switching operations in power system corrective control computations. *IEEE Trans Power Syst* 1987;2(3):669-75.
- Shao W, Vittal V. Corrective switching algorithm for relieving overloads and voltage violations. *IEEE Trans Power Syst* 2005;20(4):1877-85.
- Fisher EB, O'Neill RP, Ferris MC. Optimal Transmission Switching. *IEEE Trans Power Syst* Aug. 2008;23(3):1346-55.
- Hedman KW, O'Neill RP, Fisher EB, et al. Optimal transmission switching with contingency analysis. *IEEE Trans Power Syst* Aug. 2009;24(3):1577-86.
- Qiu F, Wang J. Chance-constrained transmission switching with guaranteed wind power utilization. *IEEE Trans Power Syst* May 2015;30(3):1270-8.
- Villumsen JC, Bronmo G, Philpott AB. Line capacity expansion and transmission switching in power systems with large-scale wind power. *IEEE Trans Power Syst* 2013;28(2):731-9.
- Han J, Papavasiliou A. The impacts of transmission topology control on the European electricity network. *IEEE Trans Power Syst* 2016;31(1):496-507.
- Ye H, Liu Y. A new method for standing phase angle reduction in system restoration by incorporating load pickup as a control means. *Int J Electr Power Energy Syst* 2013;53:664-74.
- Zhou Y, Liu Y, Hu X. Power system network reconfiguration after blackout. *Proc CSEE* 2008;10:32-6.
- Gu X, Li S, Liang H, et al. Optimization decision-making method for looped network restoration to eliminate transmission line overload in network reconfiguration. *Proc CSEE* 2017;37(5):1379-89.

- [28] Diaaeldin I, et al. Optimal Network Reconfiguration in Active Distribution Networks with Soft Open Points and Distributed Generation. *Energies* 2019;12(21): 4172. <https://doi.org/10.3390/en12214172>.
- [29] Ali, Ziad M, et al. Scenario-Based Network Reconfiguration and Renewable Energy Resources Integration in Large-Scale Distribution Systems Considering Parameters Uncertainty. *Mathematics* 2021;9(1):26. <https://doi.org/10.3390/math9010026>.
- [30] Sundar K, Nagarajan H, Roald L, et al. Chance-Constrained Unit Commitment With N-1 Security and Wind Uncertainty. *IEEE Trans Control Network Syst* Sept. 2019;6 (3):1062–74.
- [31] Li Z, Wu W, Shahidehpour M, et al. Adaptive Robust Tie-Line Scheduling Considering Wind Power Uncertainty for Interconnected Power Systems. *IEEE Trans Power Syst* July 2016;31(4):2701–13.
- [32] Zhao J, et al. Robust Distributed Coordination of Parallel Restored Subsystems in Wind Power Penetrated Transmission System. *IEEE Trans Power Syst* July 2020;35 (4):3213–23.
- [33] Xu J, et al. A day-ahead economic dispatch method considering extreme scenarios based on wind power uncertainty. *CSEE J Power Energy Syst* June 2019;5(2): 224–33.
- [34] Milligan M, et al. Wind power myths debunked. *IEEE Power Energ Mag* 2009;7(6): 89–99.
- [35] Ming Y, Cao J. Electrical Load Prediction in Energy Internet via Linear Correlation Coefficient Approach. In: 2018 IEEE International Conference on Energy Internet (ICEI), Beijing; 2018. p. 157–62.
- [36] Li Z, Wu W, Zhang B. A robust interval economic dispatch method accommodating large-scale wind power generation part two uncertainty set modeling and conservativeness adjustment. *Automat Electric Power Syst* 2014;38(21):32–8.
- [37] Dörfler F, Simpson-Porco JW, Bullo F. Electrical networks and algebraic graph theory: models, properties, and applications. *Proc IEEE* 2018;106(5):977–1005.
- [38] Christie R. 118 bus power flow test case [EB/OL]. [2016-06-19]. [http://www.ee.washington.edu/research/pstca/pf118/pg\\_tca118bus.htm](http://www.ee.washington.edu/research/pstca/pf118/pg_tca118bus.htm).

**Shaoyan Li** received the B.S. degree and Ph.D. degree in electrical engineering from North China Electric Power University (NCEPU), Hebei Province, China, in 2012 and 2017, respectively. He is currently a lecturer of electrical engineering at NCEPU. His research interests include power system security defense and restoration control, operation and optimization of power system with new energy.

**Liyuan Wang** received the B.S. degree in 2018 from Yanshan University, Hebei Province, China, and the M.S. degree in 2021 from North China Electric Power University (NCEPU), Hebei Province, China. She currently works in Changfeng County Power Supply Company of State Grid Anhui Electric Power Company Ltd. Her research interests include power system security defense and restoration control.

**Xueping Gu** received the M.Sc. degree in 1988 from Harbin Institute of Technology, Harbin, China, and the Ph.D. degree in 1996 from North China Electric Power University (NCEPU), Hebei Province, China, both in electrical engineering. He is currently a professor of electrical engineering at NCEPU. His research interests include application of intelligent technology in power system, power system security and stability, and power system restoration.

**Hanguang Zhao** received the B.S. degree in 2020 from Wuhan University of Technology, Hubei Province, China, and he is working toward the M.S. degree in North China Electric Power University, Hebei Province, China. His research interests include power system security defense and restoration control.

**Yongzhao Sun** received the B.S. degree in 2019 from Hebei University of Technology, China, and he is working toward the M.S. degree in North China Electric Power University, Hebei Province, China. His research interests include power system security defense and restoration control.